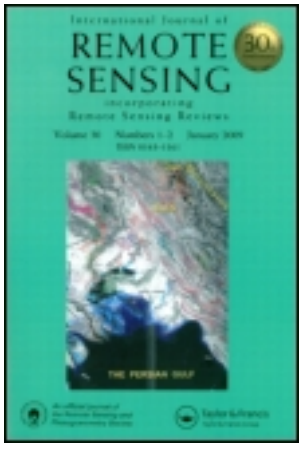

International Journal of Remote Sensing

Publication details, including instructions for authors and subscription information:
http://www.tandfonline.com/loi/tres20

Semi-automated methods for mapping wetlands using Landsat ETM+ and SRTM data

Md. A. Islam [a], P. S. Thenkabail [a], R. W. Kulawardhana [a], R. Alankara [a], S. Gunasinghe [a], C. Edussriya [b] & A. Gunawardana [b]

[a] International Water Management Institute, P.O. Box 2075, Colombo, Sri Lanka

[b] Central Environmental Authority, No. 104, Denzil Kobbekaduwa, Mawatha, Battaramulla, Sri Lanka

Published online: 07 Nov 2008.

To cite this article: Md. A. Islam, P. S. Thenkabail, R. W. Kulawardhana, R. Alankara, S. Gunasinghe, C. Edussriya & A. Gunawardana (2008) Semi-automated methods for mapping wetlands using Landsat ETM+ and SRTM data, International Journal of Remote Sensing, 29:24, 7077-7106, DOI: 10.1080/01431160802235878

To link to this article: http://dx.doi.org/10.1080/01431160802235878

International Journal of Remote Sensing
Vol. 29, No. 24, 20 December 2008, 7077–7106

Taylor & Francis
Taylor & Francis Group

Semi-automated methods for mapping wetlands using Landsat ETM+ and SRTM data

Md. A. ISLAM†, P. S. THENKABAIL*†, R. W. KULAWARDHANA†, R. ALANKARA†, S. GUNASINGHE†, C. EDUSSRIYA‡ and A. GUNAWARDANA‡

†International Water Management Institute, P.O. Box 2075, Colombo, Sri Lanka
‡Central Environmental Authority, No. 104, Denzil Kobbekaduwa, Mawatha, Battaramulla, Sri Lanka

(*Received 8 January 2007; in final form 18 May 2008*)

The overarching goal of this study was to develop a comprehensive methodology for mapping natural and human-made wetlands using fine resolution Landsat enhanced thematic mapper plus (ETM+), space shuttle radar topographic mission digital elevation model (SRTM DEM) data and secondary data. First, automated methods were investigated in order to rapidly delineate wetlands; this involved using: (a) algorithms on SRTM DEM data, (b) thresholds of SRTM-derived slopes, (c) thresholds of ETM+ spectral indices and wavebands and (d) automated classification techniques using ETM+ data. These algorithms and thresholds using SRTM DEM data either over-estimated or under-estimated stream densities (S_d) and stream frequencies (S_f), often generating spurious (non-existent) streams and/or, at many times, providing glaring inconsistencies in the precise physical location of the streams. The best of the ETM+-derived indices and wavebands either had low overall mapping accuracies and/or high levels of errors of omissions and/or errors of commissions.

Second, given the failure of automated approaches, semi-automated approaches were investigated; this involved the: (a) enhancement of images through ratios to highlight wetlands from non-wetlands, (b) display of enhanced images in red, green, blue (RGB) false colour composites (FCCs) to highlight wetland boundaries, (c) digitizing the enhanced and displayed images to delineate wetlands from non-wetlands and (d) classification of the delineated wetland areas into various wetland classes. The best FCC RGB displays of ETM+ bands for separating wetlands from other land units were: (a) ETM+4/ETM+7, ETM+4/ETM+3, ETM+4/ETM+2, (b) ETM+4, ETM+3, ETM+5 and (c) ETM+3, ETM+2, ETM+1. In addition, the SRTM slope threshold of less than 1% was very useful in delineating higher-order wetland boundaries. The wetlands were delineated using the semi-automated methods with an accuracy of 96% as determined using field-plot data.

The methodology was evaluated for the Ruhuna river basin in Sri Lanka, which has a diverse landscape ranging from sea shore to hilly areas, low to very steep slopes (0° to 50°), arid to semi-arid zones and rain fed to irrigated lands. Twenty-four per cent (145 733 ha) of the total basin area was wetlands as a result of a high proportion of human-made irrigated areas, mainly under rice cropping. The

*Corresponding author. Email: p.thenkabail@cgiar.org

International Journal of Remote Sensing
ISSN 0143-1161 print/ISSN 1366-5901 online
http://www.tandf.co.uk/journals
DOI: 10.1080/01431160802235878

wetland classes consisted of irrigated areas, lagoons, mangroves, natural vegetation, permanent marshes, salt pans, lagoons, seasonal wetlands and water bodies. The overall accuracies of wetland classes varied between 87% and 94% (K_{hat}=0.83 to 0.92) with errors of omission less than 13% and errors of commission less than 1%.

1. Introduction, background and rationale

Wetlands play an important role in bio-geochemical cycling, flood control and recharging of aquifers. They are considered to be the richest of the biomes (May *et al.* 2002), and are cradles of biological diversity that support unique flora and fauna and are very productive environments (Ramsar 2004). They serve as potential sites for aquaculture, breeding of waterfowl and significant carbon sinks (Dwivedi *et al.* 1999). During the last 15 years, the importance of wetlands and their management has gained increasing recognition in many parts of the world. Thus, a good inventory and map of wetland systems is very useful to understand the spatial distribution of different wetlands and their linkage with other land units. This will help in planning, management and conservation of wetlands. Thus, the inventorying and management of wetlands has become very important today.

Remote sensing offers the opportunity to map and inventory wetlands rapidly and consistently, irrespective of the geographic location (see Thenkabail and Nolte 1995, 1996, Thenkabail *et al.* 2000a). There are several studies (e.g. Thenkabail and Nolte 1996, Lunetta *et al.* 1999, Töyrä *et al.* 1999, Thenkabail *et al.* 2000a, Lyon 2001, Harvey *et al.* 2001, May *et al.* 2002, Ozesmi and Bauer 2002, Kulawardhana *et al.* 2007) that discuss methods of wetland mapping using remote sensing. Lunetta *et al.* (1999) showed that the wetlands in the northern United States were mapped with an accuracy of 88% using multidate Landsat-5 imagery, whereas the accuracy using the single date imagery was only 69%. However, when very fine resolution ($\leqslant$4 m) imagery from IKONOS was used, an accuracy of 88% was achieved using single date imagery (May *et al.* 2002). The combination of radar and visible/infrared satellite imagery is also effective (Töyrä *et al.* 1999). Bourgeau-Chavez *et al.* (2001) used shuttle imaging radar-C (SIR-C) data. Fully polarimetric L- and C-band data were used in hierarchical analysis and maximum likelihood classification techniques for the detection of flooding beneath vegetated canopies. Baghdadi *et al.* (2001) used C-band SAR data for mapping wetland in Africa by using supervised classification with an accuracy of 73% for a single date. There are many studies based on radar imagery, but none of these studies show if it is possible to differentiate irrigated crop field and seasonal wetland from the rest of the image by applying automated techniques on single date data. The airborne visible/infrared imaging spectrometer (AVIRIS) was also used to produce a vegetation map for a portion of the Everglades National Park, Florida, USA; this averaged 66% correct for all classes (Hirano *et al.* 2003). The studies referred to above were dependent on automated classification approaches for wetland mapping. All this literature describe how wetlands can be mapped using different methods applied with different sensors, but none of them studied how wetland can be mapped using a single date dry season image by applying semi-automated methods in order to reduce the manual work and increase the accuracy substantially.

Indeed, the most commonly used computer classification method to map wetlands is unsupervised classification or clustering (Ozesmi and Bauer 2002). However, mapping wetlands through classification is difficult because of spectral confusion

with other land cover classes and among different types of wetlands (Ozesmi and Bauer 2002). Studies (e.g. Harvey *et al.* 2001) have shown that visually interpreted wetland maps produced 9% higher accuracies than automated approaches. Generally, visual interpretation is more accurate than automated approaches. However, the visual approach is cumbersome and impractical for larger areas.

The biggest challenge in wetland mapping is wetland delineation. None of the studies reported in the previous paragraphs here deal with this adequately. Indeed, without a proper delineation, wetland classification and characterization is not possible. High levels of accuracies in delineating and mapping wetlands is feasible when multidate and/or multi-sensor and/or very high spatial resolution imagery are used (e.g. Ozesmi and Bauer 2002, Jenson *et al.* 2002, Lan and Zhang 2006). However, such studies over large areas will be very costly and time-consuming. Thereby, one of the main challenges set forth in this study is to develop methods that can provide high levels of accuracies using freely available, high quality, public domain datasets such as Landsat enhanced thematic mapper (ETM+) and space shuttle radar topography mission (SRTM) data.

Given the above background, the overarching goal of this paper is to investigate and develop comprehensive sets of automated and semi-automated methods and techniques for delineating, classifying and characterizing wetlands. The overwhelming focus will be to explore methods for rapid and accurate delineation and classification of wetlands using freely available high quality remote sensing and other secondary spatial datasets from reliable sources such as the United States Geological Survey Earth Data Center (USGS EDC) and the National Atmospheric and Space Agency (NASA). The methodology was developed and tested for the Ruhuna river basin in Sri Lanka and contributes to the methodology development component of the global wetland inventory and mapping (GWIM) project lead by the International Water Management Institute (IWMI).

1.1 *Specific objectives*

The specific objectives of the study are to:

(a) Investigate the strengths and the limitations of the automated and the semi-automated methods of mapping wetlands and determine their accuracies and errors,
(b) Evaluate capabilities offered by single date Landsat ETM+ data along with SRTM data for wetland mapping in the tropical regions and
(c) Establish wetland classes from Landsat ETM+-derived wetlands areas and determine the accuracies of mapping these wetland classes.

2. Methods

2.1 *Definition of wetlands*

The very first criterion for mapping wetlands is to have a well-understood definition. The Ramsar convention (Ramsar 2004) defined wetlands as areas of marsh, fen, peatland or water, whether natural or artificial, permanent or temporary, with water that is static or flowing, fresh, brackish or salt, including areas of marine water the depth of which at low tide does not exceed six metres. The United States Geological Survey (USGS) defined wetland as a general term applied to land areas which are seasonally or permanently waterlogged, including lakes, rivers, estuaries, and

freshwater marshes; an area of low-lying land submerged or inundated periodically by fresh or saline water (Cowardin *et al.* 1979). The US Great Lakes report to the US congress (Great Lakes Report to Congress 1994) defines wetlands as areas that are regularly saturated by surface water or groundwater and is characterized by a prevalence of vegetation that is adapted for life in saturated soil conditions (e.g. swamps, bogs, fens, marshes, and estuaries). Taking the Ramsar and USGS definitions into consideration, the wetlands mapped in this study included irrigated agriculture, fresh water bodies, salt pans, lagoons, mangroves, riparian vegetation, permanent marshes, water bodies with or without aquatic plants and seasonal wetlands.

2.2 *Study area*

The Ruhuna river basin is located in Sri Lanka (see figure 1) and has a total area of 608 000 ha. The basin is bounded by the Indian Ocean from the southern side. The elevation of the Ruhuna basin varies from sea level to 2350 m with slopes from 0° to 74°. The rainfall in the basin is bi-modal (as it is in the rest of the country) with precipitation from the two seasons each year, the north-east monsoon from December to February and the south-west monsoon from May to September. The mean annual rainfall is 1574 mm based on 30 year (1961 to 1990) data, while monthly average ranges from 48 to 274 mm (Jayatillake 2002). Mean monthly potential evapo-transpiration (PET) in upper catchments varies from 2.8 mm day^{-1} to 5.0 mm day^{-1}. The PET for lower catchments is much higher and varies from 4.6 mm day^{-1} to 6.0 mm day^{-1} (Jayatillake 2002). There are 26 major and medium reservoirs in the basin with a total storage capacity of 883×10^6 m^3. The reservoir density is 0.16×10^6 m^3 km^{-2}. Total water spread area is 7493 ha (Jayatillake 2002).

The Ruhuna basin has a diverse landscape covering a wide array of land cover such as fresh water bodies, lagoons, salt pans, mangroves, rain fed and irrigated agriculture, rivers, forests and shrub/scrub lands. People depend mainly on agriculture for their livelihood. This basin has been chosen for this study because of the diversity of the landscape and also because it is one of the benchmark basins of the IWMI.

2.3 *Satellite sensor data characteristics*

Primarily, this study used Landsat enhanced thematic mapper plus (ETM+) 30 m data for the nominal year 2000 (see table 1). Peak dry season Landsat images, for the month of April, were acquired as, during this period, the differences in uplands versus lowland wetlands are maximum. The Indian remote sensing (IRS) very fine resolution (VFR) 5 m panchromatic data was used to verify and help assist the wetland boundary delineation from Landsat ETM+. Monthly moderate imaging spectrometer (MODIS) time-series normalized difference vegetation index (NDVI) maximum value composite (MVC) at a 500 m scale for the year 2001 was used to characterize the final wetland classes. The MODIS time-series NDVI MVC composition techniques are described in detail in Thenkabail *et al.* (2005).

Some secondary data were also used to assist the wetland mapping exercise. The most useful data was the SRTM DEM at 90 m resolution. The slope map generated using the SRTM DEM was very useful to identify low lying areas. The SRTM DEM was also used for rapid automated delineation of the stream network. Extensive field-plot (GT) data, Survey department's topographic map of 1985 were also used

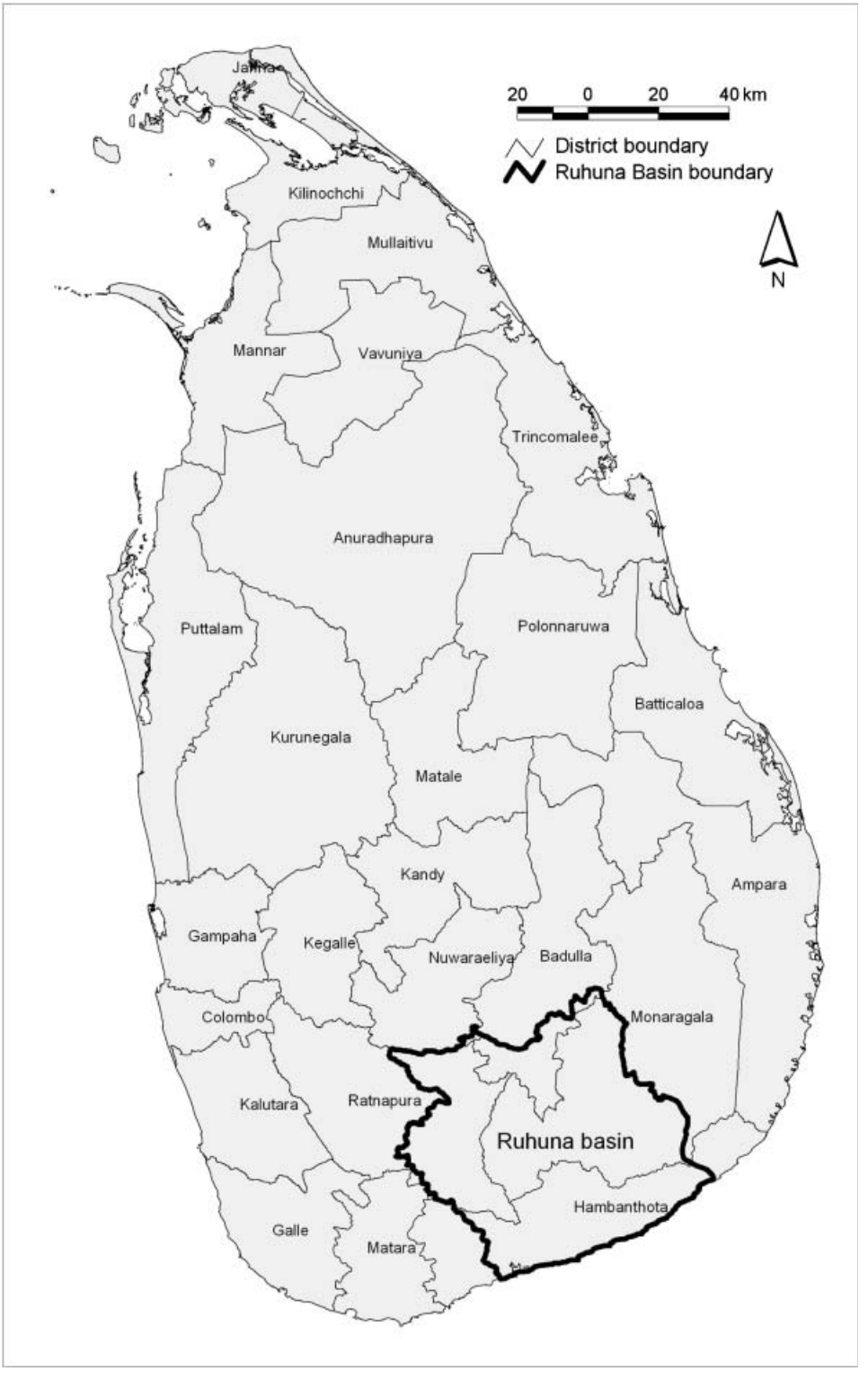

Figure 1. The location of the Ruhuna river basin (study area) in Sri Lanka.

Table 1. Characteristics of satellite sensor data used in this study.

Sensor	Spatial resolution (m)	No. of spectral bands	Radiometric depth (bit)	Band range (nm)	Band centres (nm)	Band widths (nm)	Irradiance ($W\,m^{-2}\,sr^{-1}\,\mu m^{-1}$)
1. MODIS	250, 500, 1000 m	7	8 bit	0.62 to 0.67	0.64	0.05	
				0.84 to 0.876	0.858	0.036	
				0.459 to 0.479	0.469	0.02	
				0.545 to 0.565	0.555	0.02	
				0.123 to 0.125	0.124	0.002	
				0.163 to 0.165	0.164	0.002	
				0.211 to 0.216	0.214	0.005	
2. Landsat-7 ETM+	30 m	7	8 bit	0.45 to 0.52	0.482	0.65	0.1970
				0.52 to 0.60	0.565	0.80	0.1843
				0.63 to 0.69	0.66	0.60	0.1555
				0.50 to 0.75	0.625	0.15	0.1047
				0.75 to 0.90	0.825	0.20	0.2271
				10.0 to 12.5	11.45	2.50	
				1.55 to 1.75	0.165	0.26	0.8053
3. IRS-1D-Panchromatic	5.6 m	1	8 bit	0.50 – 0.75	0.63	0.25	

to confirm wetland boundaries along with IRS 5 m data. Precipitation data from East Anglia University's Climatic Research Unit (CRU) at 50 km resolution helped in understanding the rainfall pattern.

2.4 *Ground-truth data characteristics*

A ground-truth survey was conducted during 15 to 30 May 2005, which is very close to the image acquisition month (April). For such a big basin, a random and systematic survey is unrealistic and costly. Therefore, the sampling was carried out based on the accessibility through road networks and footpaths. A sampling unit was set as 30 m. Class labels were assigned in the field using a system that allows merging to a higher class, or breakdown into a distinct class, based on the land cover percentage taken at each location (Thenkabail *et al.* 1995, 1996). Class names were kept as descriptive as possible. A total of 255 global positioning system (GPS) coordinates were taken in the Ruhuna basin area (figure 2) including detailed descriptions and percentage of land cover types and digital photographs. The GPS coordinates were taken in the universal transverse mercator (UTM), zone 44N and the geographic coordinate system (latitude–longitude). The data points were almost exclusively on lowland wetlands (see figure 2). Of these 255 field-plot points, 230 points were for lowland wetlands and the remaining 25 for other land units. One in two points collected on wetlands were reserved for accuracy assessment, leaving 115 points to be used for class identification and labelling process.

2.5 *Automated methods of wetland boundary delineation*

The automated methods (figure 3) for delineating wetland boundaries were attempted using: (a) algorithms on SRTM DEM data, (b) thresholds of SRTM derives slopes, (c) thresholds of spectral indices and wavebands and (d) automated classification techniques.

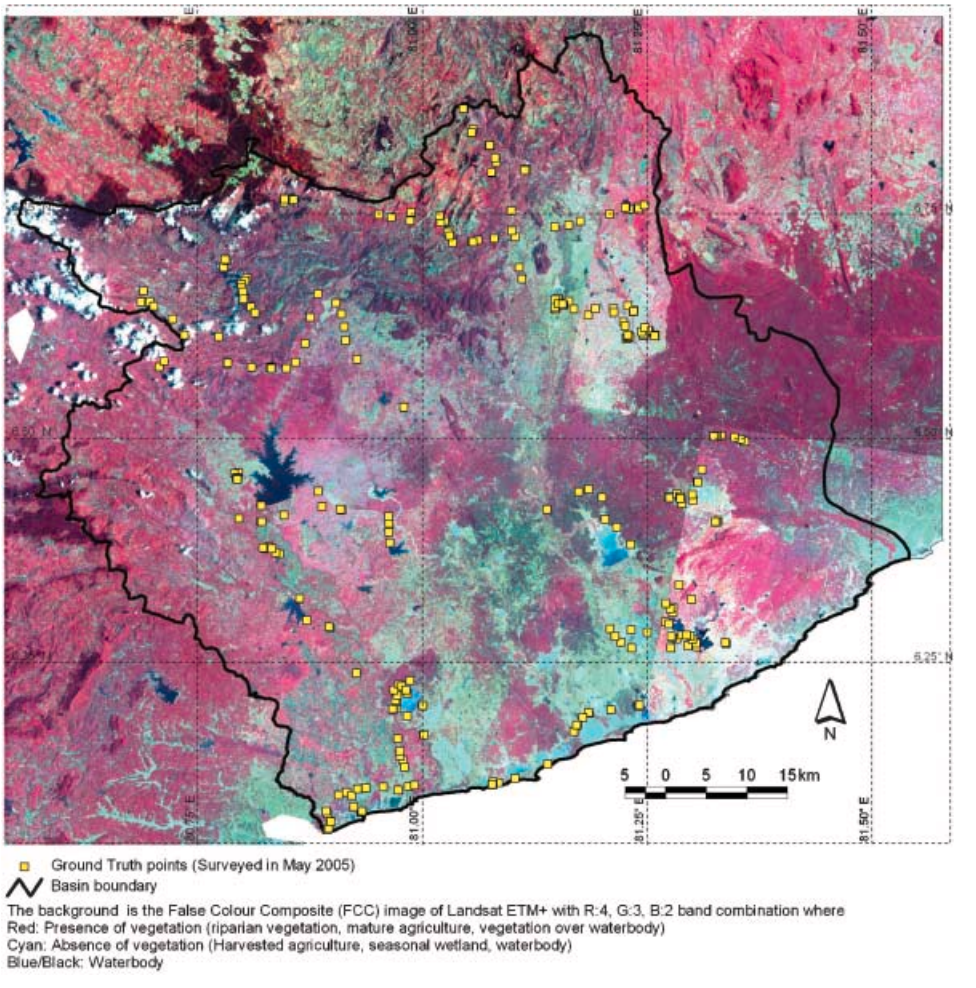

Figure 2. The field-plot data points used to identify wetland areas and to determine wetland classes are overlaid on the Landsat ETM+ false colour composite red, green, blue 4, 3, 2.

2.5.1 Algorithms on SRTM DEM data. The wetlands are topographical lowlands and hence the DEM data offers a fine opportunity to delineate lowlands from uplands through the automated approaches discussed below. Delineating wetlands using DEM is a two-step procedure. First, the drainage system, which is part of the wetland system, is automatically delineated using algorithms. Second, the areas on either side of the drainage system consist of valley bottoms and hydromorphic valley fringes, both of which are part of the wetland areas. The valley bottoms and the hydromorphic valley fringes are then delineated by proximity analysis by taking the drainage system as centre and spreading certain distance (discussed below) on either side of the drainage system.

The drainage system was delineated using SRTM DEM data by using appropriate algorithms, as described below, in ArcGIS (ESRI 2001) and following a set of topographical functions. The process involved:

(i) Filling sinks. A sink is a cell or set of spatially connected cells whose flow direction cannot be assigned to one of the eight valid values in a flow

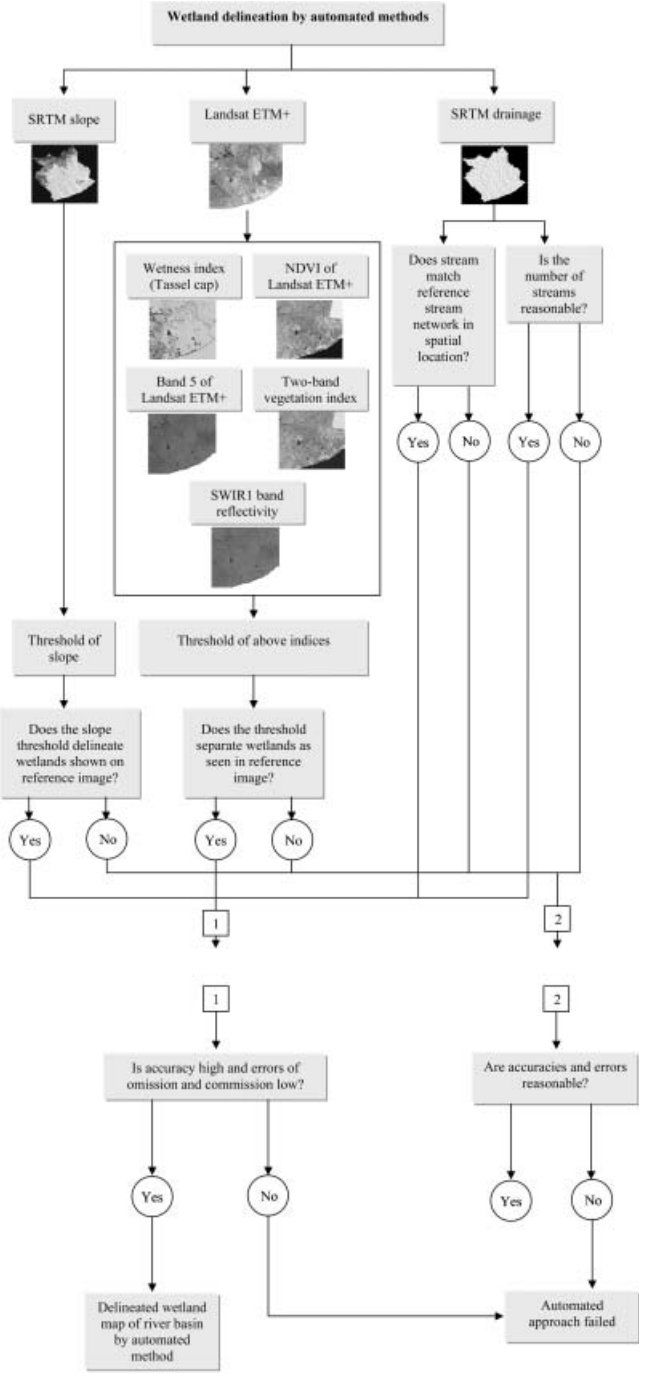

Figure 3. The methodology flow chart for the automated wetland delineation.

direction grid. This can occur when all neighbouring cells are higher than the processing cell, or when two cells flow into each other creating a two-cell loop (ESRI 2001). All the sinks of the DEM were filled up by using

the FILL function of the ArcInfo Grid module. An eight cells neighbourhood, which delineated drainage, was used for this function. It is a iterative process that goes to each cell and fills the sinks by comparing the value of neighbouring cells until all the sinks are filled.

(ii) Generation of flow direction. The direction of flow is determined by finding the direction of steepest descent from each cell. This is calculated as: drop=(change in z value)/(distance) $\times$ 100. The distance is determined between cell centres. Therefore, if the cell size is 1, the distance between two orthogonal cells is 1 and the distance between two diagonal cells is 1.414. If the descent to all adjacent cells is the same, the neighbourhood is enlarged until a steepest descent is found (ESRI 2001). The function FLOWDIRECTION was used to calculate the direction of flow of each cell. The DEM was assigned as input for this function.

(iii) Generation of flow accumulation. Flow accumulation represents the accumulated flow in each grid cell. It is calculated by using flow direction and by counting the number of cells flowing to a particular cell. Thus, flow accumulation represents the number of upstream cells of any cell in an area. The FLOWACCUMULATION function was used to calculate this automatically while it takes the flow direction grid as input.

(iv) Generation of stream network. A set of thresholds of 10, 25, 50, 75, 100 and 500 pixels were used to generate stream network. All the cells in the flow accumulation grid that are above or equal to those threshold values were identified to get raster linear networks. The output grids were then vectorized by using the STREAMLINE function of ArcInfo, which takes raster linear networks and flow direction rasters as input to produce linear vectors that also show the direction of flow (node-to node properties of each stream link are maintained towards the direction of flow).

The above methods lead to generating a stream network for the Ruhuna river basin (figure 4). Once the streams are accurately derived, the wetland areas were delineated using a buffer that maps valley bottoms and hydromorphic valley fringes (Thenkabail *et al.* 1996), which adjoin either side of the drainage network. However, there was great uncertainty in this estimation as precise knowledge on the width of the valley bottoms and fringes is lacking.

2.5.2 Thresholds on SRTM DEM-derived slopes. The SRTM DEM data was used to derive a local slope map (in degrees) using the SLOPE function of the ArcInfo Workstation GIS. A threshold (see table 3) of degree slope provides areas of wetlands or low laying areas (figure 4) and non-wetlands.

2.5.3 Thresholds of spectral indices and wavebands. First, the wetlands in the images are highlighted by enhancing images (Lyon *et al.* 1998, Lunetta *et al.* 1999). Second, the thresholds of indices and wavebands will automatically delineate wetlands from non-wetlands (Lyon *et al.* 1998, Hirano *et al.* 2003, Schowengerdt 2007). Since the enhancement techniques are the same for the automated and semi-automated techniques, we will discuss the specific indices and wavebands and their thresholds for separating wetlands from non-wetlands in §2.6.1 (table 3).

2.5.4 Automated classification techniques. Over the years, numerous researchers have attempted wetland separation through automated classification techniques on various remotely sensed data (see Lyon 2001, Campbell 2002, Jensen *et al.* 2002,

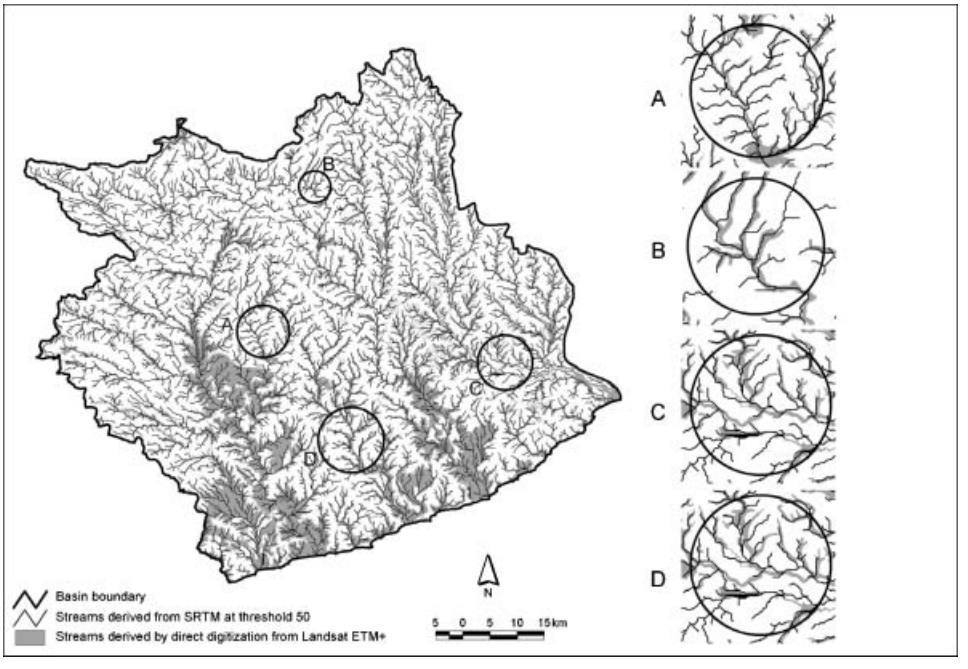

Figure 4. An algorithm was written in ArcGIS to automatically delineate the drainage network. The network so delineated is overlaid on the Landsat ETM + derived wetlands.

Fuller *et al.* 2006, Lan and Zhang 2006) without first delineating wetland areas from other land units (§2.6). However, Ozesmi and Bauer (2002) show the difficulties of wetland classification because of spectral confusion with other land cover classes and among different types of wetlands. Since the automated classification techniques are applied on entire image areas that include wetlands and other land units, classification accuracies improve when multi-temporal data are used (Ozesmi and Bauer 2002), or through geographic information system (GIS) modelling techniques are used (Sader *et al.* 1995), along with ancillary data such as soils and topography (Ozesmi and Bauer 2002), or when data from multiple sensors (Lyon 2001) are used, or very fine resolution imagery (e.g. Fuller *et al.* 2006) and/or classification is performed using fused data from multiple sensors and secondary data (see Thenkabail *et al.* 2006). In this study, attempts were made to use various classification approaches (Jensen *et al.* 1995, Lyon 2001, Campbell 2002, Ozesmi and Bauer 2002), but the confusion amongst wetland classes (table 4) and between wetlands and non-wetlands (Lan and Zhang 2006; table not presented here) were highly significant, discouraging the use of automated classification approaches.

2.6 *Semi-automated methods of wetland boundary delineation*

The semi-automated methods (figure 5) involved: (a) enhancement of images through ratios to highlight wetlands from non-wetlands, (b) display of enhanced images in red, green, blue (RGB) false colour composites (FCCs) to highlight wetland boundaries, (c) digitizing the enhanced and displayed images and delineate wetlands from non-wetlands and (d) classification of the delineated wetlands areas into various wetland classes. The process is described in detail below.

Table 2. Delineation of stream densities and stream frequencies using: (a) SRTM data, (b) topographic maps and (c) Landsat ETM+ imagery.

Serial no.	Data type	Threshold* (Dimensionless)	Stream density (S_d) (km km^{-2})	Stream frequency (S_f) (no. km^{-2})	Wetland area factor (WAF) Wetland area (km^2) / Total basin area (km^2) (Dimensionless)
A. SRTM data					
1	Stream-SRTM	10	2.46	5.96	–
2	Stream-SRTM	25	1.57	2.46	–
3	Stream-SRTM	50	1.14	1.27	–
4	Stream-SRTM	75	0.94	0.86	–
5	Stream-SRTM	100	0.82	0.66	–
6	Stream-SRTM	500	0.38	0.13	–
B. Topographic maps (1 : 50 000)					
1	Stream-Topo map 1 : 50 000	–	1.05	1.13	–
2	Stream-Topo map 1 : 250 000	–	0.60	0.29	–
C. Landsat imagery					
3	Landsat-7	–	0.54	0.24	0.24

Note: * is the threshold for SRTM and implies the minimum number of upstream cells chosen to constitute a stream.

Table 3. Automated methods of delineating wetlands. Thresholds of Landsat ETM+ indices and wavebands as well as SRTM derived slope threshold for delineating wetlands.

Index and band for automatic delineation	DN (threshold value)	Accuracy[1] (%)	Error	
			Commission[2] (%)	Omission[3] (%)
1. Tassel cap wetness index (TCWI)				
Wetness-Tcap (Dimensionless)	0 to 5	83	305	17
	6 to 10	5	8	95
	11 to 20	4	4	96
	21 to 40	7	0.4	93
	41 to 60	1	0	99
	61 to 80	1	0	100
	81 to 100	0	0	100
	101 to 120	0	0	100
	121 to 140	0	0	100
	141 to 160	0	0	100
	161 to 180	0	0	100
	181 to 190	0	0	100
2. Two band vegetation index (TBVI)[4]				
$TBVI_{32}$	−1 to −0.25	73	15	97
$TBVI_{42}$	−1 to 0.35	78	11	81
$TBVI_{43}$	−1 to 0.3	78	6	85
$TBVI_{52}$	−1 to 0.1	78	6	87
$TBVI_{53}$	−1 to 0.3	78	11	81
$TBVI_{57}$	−1to 0.25	75	19	88
$TBVI_{72}$	−1 to −0.3	75	22	83
$TBVI_{73}$	−1 to −0.1	75	23	79
3. NDVI				
NDVI (Dimensionless −1 to +1)	−1 to −0.5	2	0	98
	−0.5 to 0	23	19	77
	0 to 0.1	15	34	85
	0.1 to 0.2	21	75	79
	0.2 to 0.3	25	112	75
	0.3 to 0.4	13	69	87
	0.4 to 0.5	1	8	99
	0.5 to 0.6	0	0.1	100
4. Band reflectivity[4]				
Band5 (digital number 0 to 255)	1 to 5	0	0	100
	6 to 10	0	0	100
	11 to 20	5	0	95
	21 to 40	3	2	97
	41 to 60	6	18	94
	61 to 80	25	88	75
	81 to 100	27	124	73
	101 to 120	16	60	84
	121 to 140	10	17	90
	141 to 160	5	5	95
	161 to 180	2	2	100
	181 to 200	1	1	100
	201 to220	0	0	100
	221 to 255	0	1	100

Table 3. (*Continued*).

Index and band for automatic delineation	DN (threshold value)	Accuracy[1] (%)	Error	
			Commission[2] (%)	Omission[3] (%)
5. SRTM-derived slope				
Slope (°)	0 to 0.5	28	24	72
	0.5 to 1	24	53	76
	1 to 2	29	97	71
	2 to 3	8	27	92
	3 to 4	2	10	98
	4 to 5	1	7	99
	5 to 10	3	30	97
	10 to 20	3	45	97
	20 to 40	1	24	99
	40 to 75	0	1	100

Note:
1=Accuracy=Percentage of wetland area falling inside wetland boundary;
2=Commission=Percentage of wetland area falling outside wetland boundary;
3=Omission=Percentage of wetland area not mapped as wetland by specific threshold;
4=Results of only the best performing index or waveband have been reported.

2.6.1 Enhancement of images through ratios. Various image enhancement techniques involving ratio indices were investigated for delineating wetlands automatically through simple thresholding (table 3). Numerous ratios (Lyon *et al.* 1998, Thenkabail and Nolte 1996, 2000a, Thenkabail and Nolte 2000) were investigated. The best performing indices are reported below.

(i) Tasselled cap wetness index (TCWI). The TCWI is known to be sensitive to moisture and wetness (Crist *et al.* 1984). Taking advantage of this, a TCWI image was computed using the equation (Crist *et al.* 1984):

$$\text{TCWI}=0.1509B_1+0.1973B_2+0.3279B_3+0.3406B_4-0.7112B_5-0.4572B_7, \quad (1)$$

where B_1, B_2, B_3, B_4, B_5 and B_7 are the Landsat ETM+ reflective band numbers.

(ii) Two-band vegetation indices (TBVIs). Various two-band vegetation indices were investigated for highlighting wetness and moisture. For Landsat ETM+ 7 band data, there are 21 unique TBVIs (see Thenkabail *et al.* 2000b, 2002):

$$\text{TBVI}_{ij}=\left(R_j-R_i\right)/\left(R_j+R_i\right) \quad (2)$$

where i, j=1, N, (with N=number of bands=7 for Landsat ETM+ multispectral) and R is the reflectance of the bands. A total of 49 TBVIs were computed for the Landsat band matrix of seven bands by seven bands. The indices above the diagonal are a transpose of the indices below the diagonal. Hence, after reducing for this redundancy, only 21 unique indices will be left. The normalized difference vegetation index (NDVI) is one of the TBVIs. Each TBVI was subjected to variable thresholds to get the separability of wetlands from other land units (table 3).

(iii) Band reflectivity. Similar to TBVIs, thresholds of Landsat ETM+ band reflectivity for the six non-thermal bands were used to automatically

Table 4. Error matrix showing spectral mixing between various wetland classes.

Wetland types	Irrigated harvested	Irrigated mature	Flood irrigated	Riparian vegetation	Water bodies	Seasonal wetlands	Wetland with vegetation	Mangrove	Total
Irrigated harvested	–					Y			1
Irrigated mature		–		Y			Y	Y	3
Flood irrigated			–		Y	Y		Y	3
Riparian vegetation		Y		–			Y	Y	3
Water bodies			Y		–	Y			2
Seasonal wetlands	Y		Y		Y	–			3
Wetland with vegetation		Y		Y			–		2
Mangrove		Y	Y	Y				–	3
Total	1	3	3	3	2	3	2	3	20

Note: Y indicates the presence of conflict between classes.

delineate wetlands from other land units (table 3). The optimal thresholds were determined by trial and error.

2.6.2 Display of enhanced images in RGB FCCs to highlight wetlands. Image display techniques are crucial to highlight wetlands from other land units so that the wetland boundaries are crystal clear and can be digitized accurately. The process begins by choosing the enhanced images (§2.6.1) and depicting them in various RGB FCCs. The following display of RGB FCCs distinguished the wetland boundaries from uplands the best:

- ETM + 4/ETM + 7, ETM + 4/ETM + 3, ETM + 4/ETM + 2,
- ETM + 4, ETM + 3, ETM + 5,
- ETM + 7, ETM + 4, ETM + 2 and
- ETM + 3, ETM + 2, ETM + 1,

where ETM + stands for the enhanced thematic mapper plus sensor of the Landsat-7.

The process of highlighting and distinguishing the wetlands from other land units is depicted in figure 5(*b*) and 5(*c*) for a very small sub-area of the study region. Figure 5(*c*) highlights the wetlands from non-wetlands as depicted using Landsat ETM + ratios ETM + 4/ETM + 7, ETM + 4/ETM + 3, ETM + 4/ETM + 2, displayed as a FCC in RGB.

2.6.3 Digitizing the enhanced and displayed images to delineate wetlands from non-wetlands

Once the images are enhanced (§2.6.1) and displayed (§2.6.2) at full pixel resolution (e.g. figure 5(*b*)), they are digitized directly off screen. The process of digitizing begins by selecting FCC RGBs that separate out wetlands from other land units as illustrated in figure 5. This is followed by using the additional FCC RGB combinations (e.g. ETM + 3, ETM + 2, ETM + 1) to see whether any additional wetland areas can be added that were missing from earlier FCC RGB combinations (e.g. ETM + 3, ETM + 2, ETM + 1). In addition, thresholds of SRTM-derived slopes (§2.5.2) and waveband reflectivity (§2.5.3) were used to detect the wetland boundaries.

After digitization the preliminary wetland boundary, the map was rechecked and necessary editing was carried out to correct inclusion or exclusion errors based on extensive field-plot knowledge (figure 2).

2.6.4 Classification of delineated wetland areas into wetland classes

Once the wetland boundaries are determined (§2.6.1 through to §2.6.3), the wetland areas were delineated using the Landsat ETM + data and classified using the unsupervised ISOCLASS clustering algorithm (ERDAS 2006). The ISOCLASS clustering provided a substantial within-class variance for wetlands, as also determined by Friedl *et al.* (2000) and McIver and Friedl (2002), and hence was used as a 'starting block' for determining unique wetland classes. An initial 250 classes were reduced to 15 and 8 classes through a rigorous class identification and labelling process (see figure 6; also see Thenkabail *et al.* 2006).

Classes were labelled (table 6) based on bi-spectral plots, NDVI values of classes, field-plot points and visual interpretation of 5.6 m IRS panchromatic data. It was

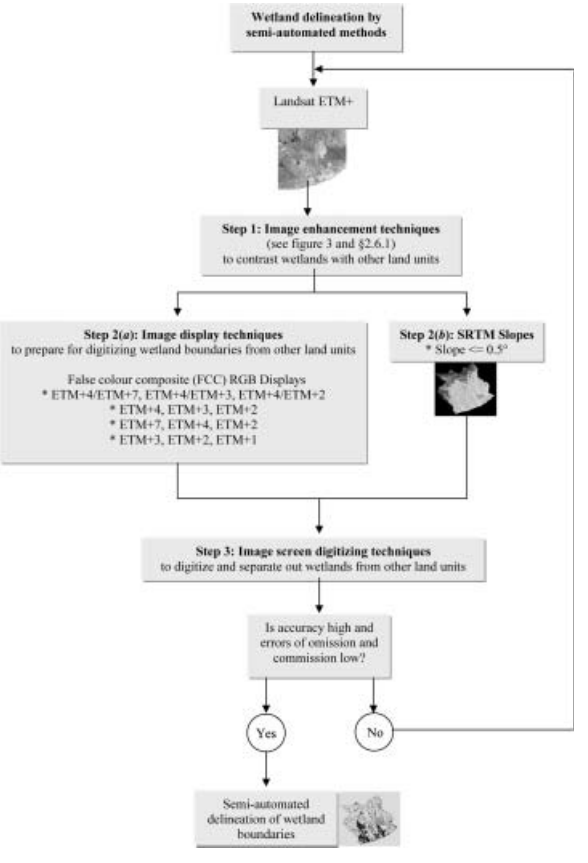

(*a*)

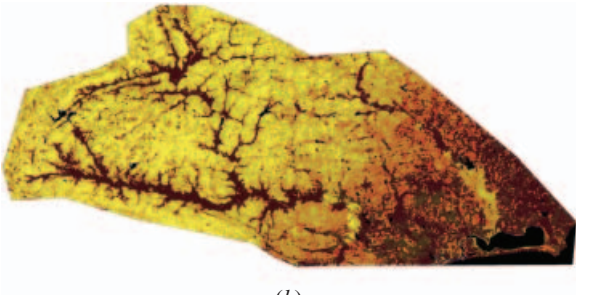

(*b*)

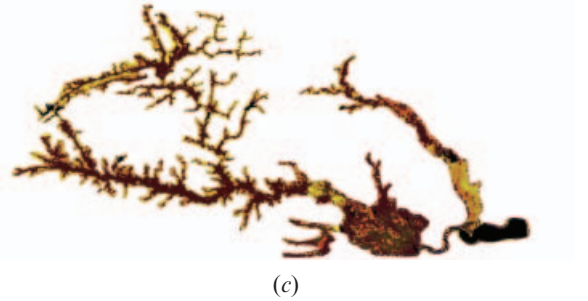

(*c*)

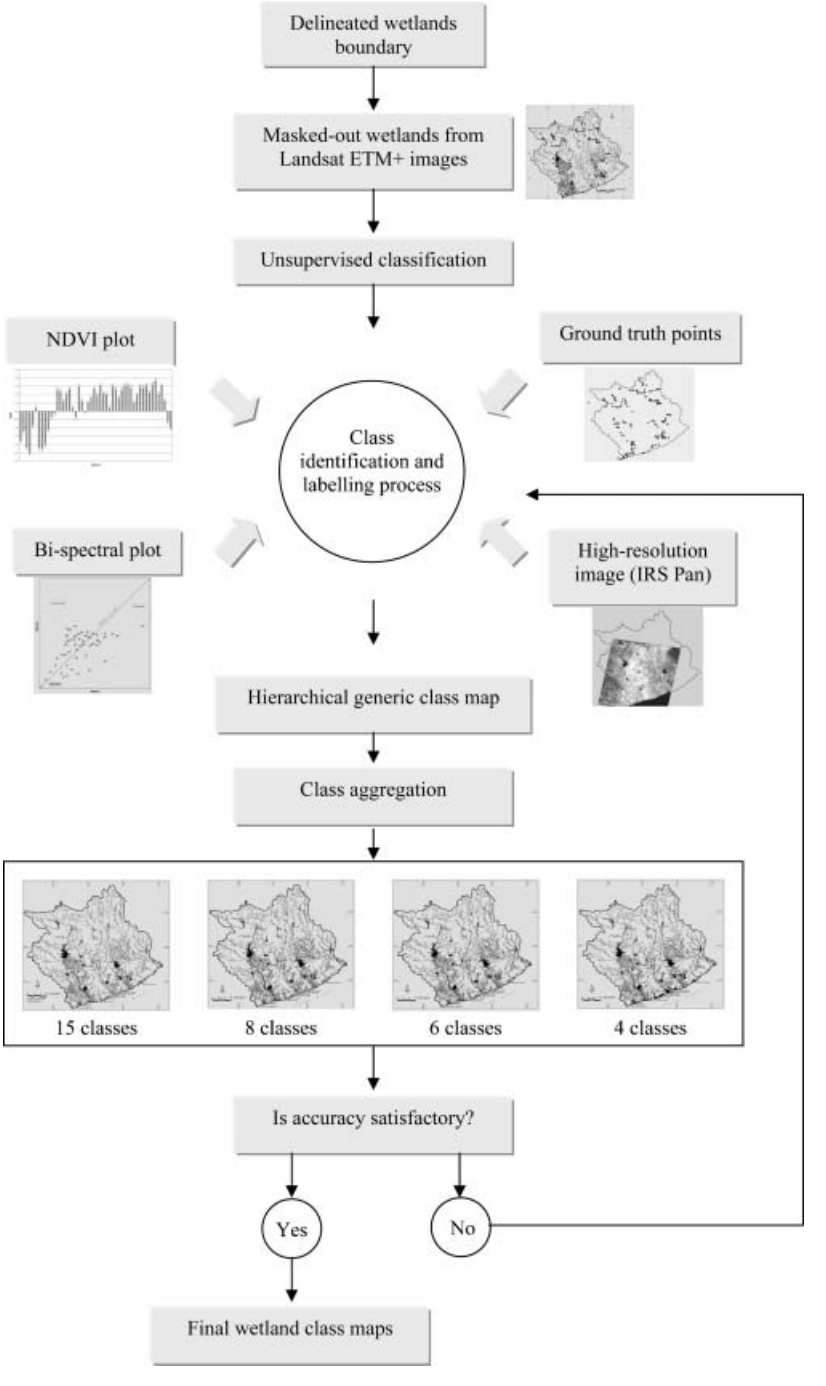

Figure 6. Illustration of wetland classification and class identification processes.

Figure 5. Semi-automated methods for wetland delineation: (*a*) methodology flow chart for the semi-automated wetland delineation, (*b*) enhancement and display to highlight wetlands depicted here in the FCC RGB of TM4/TM7, TM4/TM3, TM4/TM2 for a small sub-area in the study region and (*c*) delineated wetlands.

found that considerable numbers of class signatures were not separable because they were showing the same reflectivity in all bands.

One of the objectives of the research was to determine as many wetland classes as possible. During the class identification and labelling process (figure 6) many classes remained mixed. In order to understand the mixing process, a conflict matrix was developed that showed which classes mixed with which other classes (table 4). The classes that mixed with one another included: (a) irrigated grownup rice mixing with riparian vegetation, (b) mangrove and water bodies with densely populated aquatic plants (which also has high NDVI), (c) irrigated fields under preparation with marshy land or shallow water and (d) seasonal wetlands (which were dry for that date) with harvested agricultural fields.

In order to overcome the spectral mixing of classes that lead to conflict classes (table 4), block analysis was performed by splitting the wetland areas into: (a) irrigated agriculture including homestead, (b) water bodies and (c) riparian vegetation and mangroves. Classification (§2.6.4) and class identification and labelling process (figure 6; Thenkabail *et al.* 2006) were then performed on each block. To remove unwanted scattered pixels, the MAJORITY function was applied on a 3×3 pixel neighbourhood (ERDAS 2006). This process lead to classifications at most disaggregated (15 classes) to most aggregated (4 classes) classes (table 6). The classes followed the Ramsar wetland convention scheme.

3. Results and discussions

First, the results and discussions of mapping wetlands using automated methods are presented. This is followed by wetland mapping using semi-automated methods, computation of wetlands areas, accuracies of delineated wetlands and accuracies of wetland classes mapped. Finally, there is a discussion on the characterization of wetland classes.

3.1 *Mapping wetlands using automated methods*

The results of delineation of wetlands using automated methods (see §2.5 and its sub-sections) are presented in tables 2 and 3 and figures 4, 7(*b*) and 7(*c*).

First, the results of the use of algorithms on the SRTM DEM for delineating wetlands (see table 2 and figure 4). The overwhelming proportions of the wetlands in any landscape are along the drainage system, with drainage forming the centre of it. So, an accurate delineation of drainage is the first step towards mapping the wetland areas accurately. Once the drainage is mapped accurately, GIS techniques such as SEARCH and SPREAD can be used to map valley bottom and hydromorpic valley fringe wetland areas on either side of the stream network (see Thenkabail *et al.* 2000a, Thenkabail and Nolte 1996, 1995). The drainage indicators are measured using stream density (S_d) and stream frequency (S_f) (see table 2). The SRTM-derived S_d and S_f vary widely depending on the threshold (minimum number of upstream pixels chosen to form a stream), as seen in table 2. The advantage of the SRTM-derived drainage is the rapidity with which they are derived using automated algorithms. This can be done within a few hours of computing with a powerful computer for an entire river basin such as the one used in this study area. Once the streams are generated (figure 4), the stream density (km km^{-2}) and stream frequency (number km^{-2}) are determined and compared with the stream density (S_d) and stream frequency (S_f) generated using topographic maps (figures 7(*a*) and 7(*b*)) and

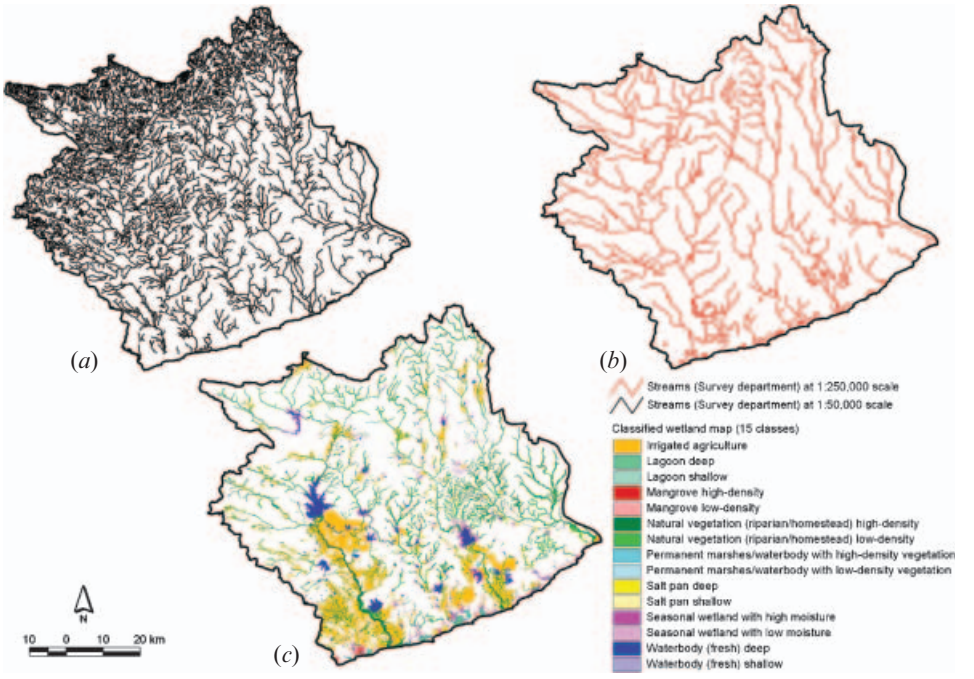

Figure 7. Delineated wetlands using Landsat ETM+ (*c*) compared with drainage network delineated using 1 : 50 000 topo maps (*a*) and 1 : 250 000 topo maps (*b*).

Landsat ETM+ images (figure 7(*c*) and table 2). Streams from topographic maps were obtained by direct digitization. The streams from Landsat imagery were also obtained by direct digitization on the image (see §§3.2 and 2.6). Later density was calculated by dividing the stream length (km) by total basin area (km^2). Frequency was calculated by dividing the number of streams by the total area of the basin (km^2). Once the streams are accurately derived, the wetland areas can be delineated using a buffer- or pixel-based majority function coupled with spatial modelling in the GIS framework in an ArcInfo Workstation GIS. The S_d and S_f generated from the SRTM DEM are compared with that of the topographic maps (figures 7(*a*) and 7(*b*)) and Landsat ETM+-generated S_d and S_f (figure 7(*c*) and table 2). When the SRTM DEM threshold was 50, the S_d values with 1.14 km km^{-2} and S_f values with 1.27 km km^{-2} were close to the corresponding reference values from topographic maps at 1 : 50 000. However, the four main problems associated in using the SRTM DEM data for wetland delineation (see figure 4) are:

(i) Spurious streams. Generation of spurious stream networks wherein significant number of streams are generated along non-existence flow paths.
(ii) Non-smooth stream alignment. Where the streams look like a connected series of straight lines coming from various directions. The Landsat ETM+ (900 m^2) has nine times better resolution than the SRTM DEM (8100 m^2), which causes the zigzag patterns seen on the SRTM data.
(iii) Spatial dislocation of streams. Streams get spatially dislocated leading to inland wetlands being mapped in areas away from their actual location.
(iv) Stream width absence. The actual wetland areas such as flood plains, inland valley bottomlands and hydromorphic fringes are represented by stream

width. Absence of and/or inadequate representation of stream widths mean that the wetland areas are inadequately represented and/or may go missing completely. The linear features seen in figure 4 are the drainages derived using the SRTM DEM.

Second, the thresholds of the SRTM slopes had low accuracies and high errors of omission and commissions (point 5 in table 3). Typically, a slope of less than 1° delineates the higher stream order or large size wetlands well, but misses out the lower order streams and associated inland valleys (see Thenkabail *et al.* 2006), leading to high omission errors (table 3). Also, the problem with the SRTM is that it does not work well in plain areas, where incorrect stream alignment is very usual.

Third, a rapid means of wetland boundary delineation will be to use thresholds of various indices (table 3). Wide arrays of such indices were investigated in this study, the best of which are reported in table 3, and which showed low accuracies and high levels of errors of omissions and/or commissions in delineating wetlands, confirming the difficulties of indices as a direct measure of wetland mapping, as indicated in Ozesmi and Bauer (2002). For example, the TCWI with a threshold of 0% to 5% provided an accuracy of 83% with errors of omission of 17% and errors of commission of 305%. The high level of errors of commission indicates non-wetlands added to wetlands.

Fourth, classification of images to delineate wetlands showed a spectral mixing between various wetlands (table 4) and between wetlands and other land units (results not shown). For example, mangroves mixed with riparian vegetation, well-grown irrigated crops, and flooded irrigated classes. Spectral mixing with other wetland classes is shown in table 4.

The above results clearly imply that automated methods have serious limitations in delineating and mapping wetlands from other land units.

3.2 *Mapping wetlands using semi-automated methods*

3.2.1 Delineation of wetlands using semi-automated methods. In the semi-automated approaches, the images were first enhanced using various ratios (see §2.6.1), displayed (§2.6.2) and digitized (§2.6.3). For example, the enhancement and zoom in display of FCC in RGB of ratios TM4/TM7, TM4/TM3 and TM4/TM2 are depicted in figure 5(*b*), highlighting the value of indices in wetland mapping (Lyon *et al.* 1998, Lunetta *et al.* 1999, Lyon 2001). This is followed by digitizing the wetlands that are seen in darker shades following the drainage system (figure 5(*b*)). The digitized wetlands are then masked and separated out of other land units (figure 5(*c*)). A similar procedure was used to delineate the wetlands of the entire river basin, leading to a map of wetland areas for the Ruhuna river basin (figure 8). The digitized wetland boundary map was rechecked using VFR IRS 5 m panchromatic data as a backdrop and editing was done to correct inclusion or exclusion errors. Slopes of less than 1° were effective to give an indication of low lying areas and hence were also used as a backdrop to check the wetland boundaries delineated using Landsat based indices and waveband reflectivity displayed as FCC RGB and then digitized. The delineation was in itself a rapid process (it took 5 days for one analyst to separate the wetlands in the total basin area of 608 000 ha).

3.2.2 Areas of wetlands delineated by semi-automated methods. The total area of the wetlands was 145 731 ha (figures 7(*c*) and 8), which is 24% of the total basin area. This is a large percentage compared to 9% to 18% in the African savannas and

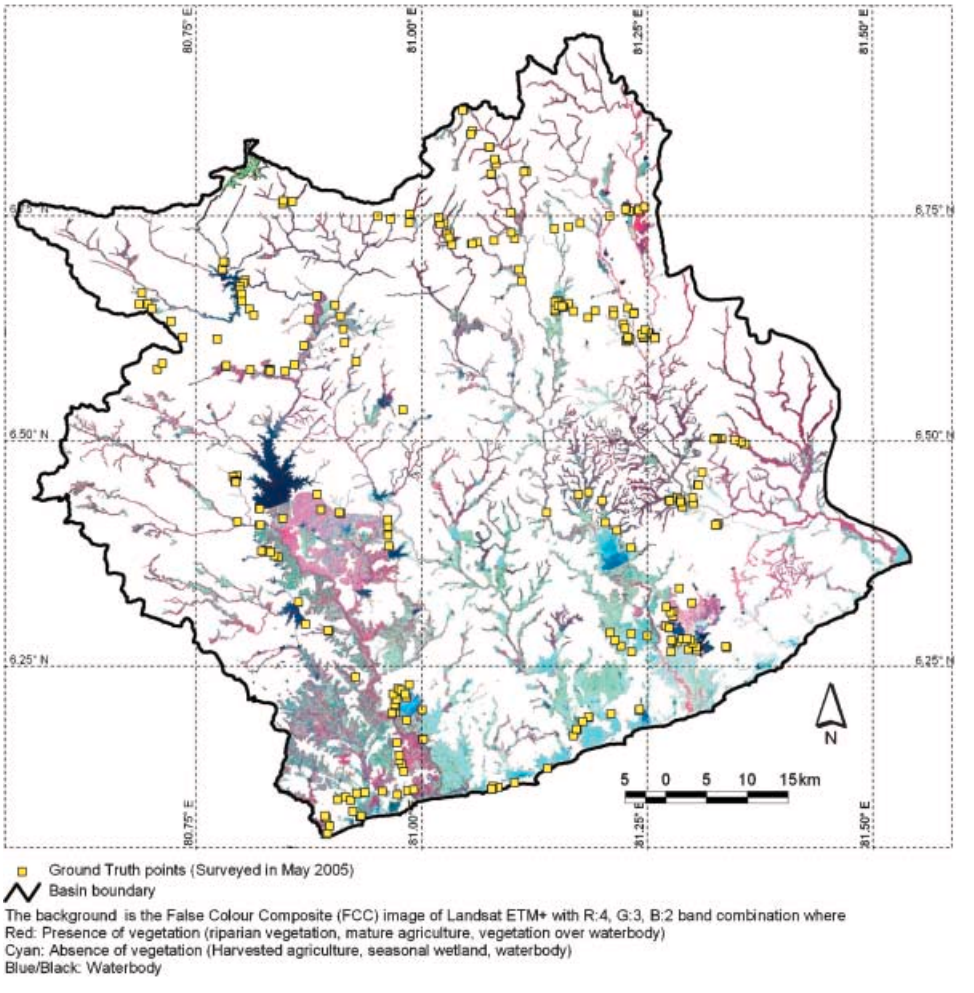

Figure 8. Verification of delineated wetlands by semi-automated methods. The field-plot data points are overlaid on Landsat ETM + delineated wetlands.

rainforests as determined by Thenkabail *et al.* (2000a), Thenkabail and Nolte (1995, 1996) and 12% in the Southern African Limpopo river basin (Kulawardhana *et al.* 2007). This is because, in the Ruhuna the irrigation extent is very high indeed, 41.5% (figure 9) of the total wetland area. If we leave the irrigated areas out, the wetland areas in the Ruhuna is 14%. The results highlight the ability of the semi-automated methods in delineating the human-made wetlands (irrigated areas) as well as natural wetlands.

3.2.3 Accuracies of wetland boundaries delineated by semi-automated methods. The delineation of wetland areas (figures 7(*c*) and 8) by semi-automated methods took place before visiting the field for collecting the field-plot data. During the field-plot data collection mission, exact coordinates of 230 wetland locations were determined using GPS and overlaid on the wetlands delineated (figure 8) using semi-automated methods. Since all the field-plot data points were gathered only after delineating wetlands, these points made a perfect independent dataset to test the accuracy of the mapping. Of the 230 field-plot points, 222 fell within the delineated wetlands (see

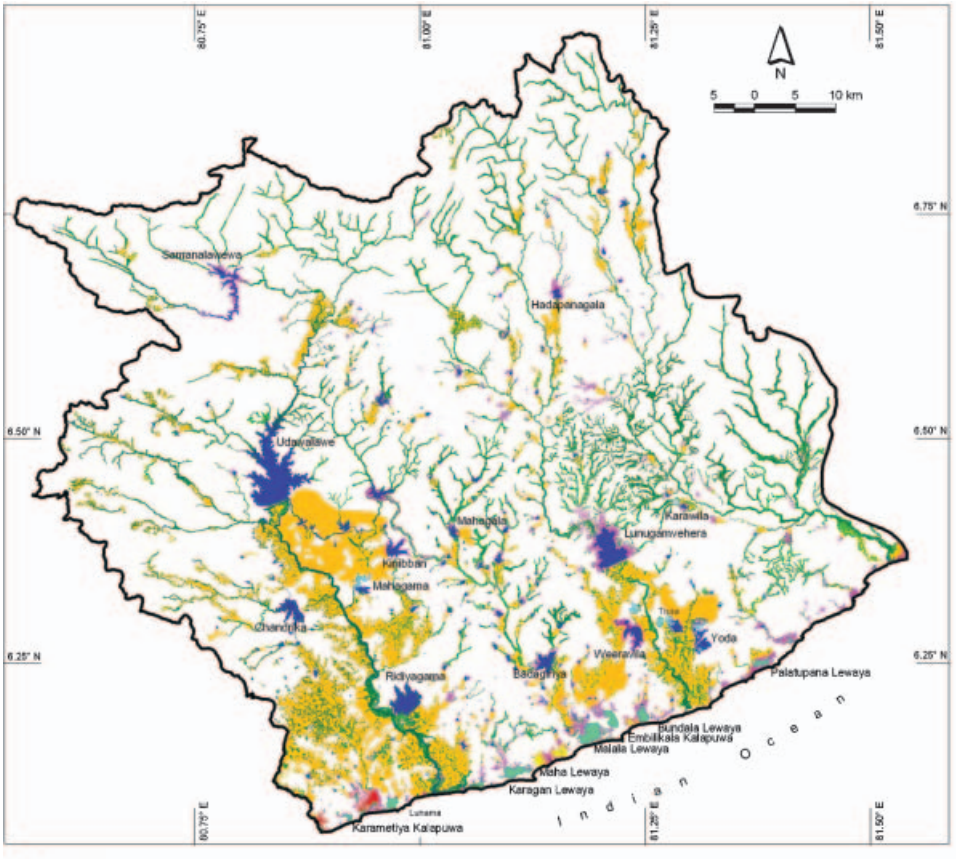

Basin boundary

Wetland types	Average NDVI (Dimensionless)	Area (Hectares)	Percentage
Irrigated agriculture	0.1	60406	41.5
Lagoon deep	−0.4	1759	1.2
Lagoon shallow	−0.1	382	0.3
Mangrove high-density	0.3	372	0.3
Mangrove low-density	0.1	252	0.2
Natural vegetation (riparian/homestead) high-density	0.3	31614	21.7
Natural vegetation (riparian/homestead) low-density	0.2	21428	14.7
Permanent marshes/waterbodies with high-density aquatic plants	0.4	323	0.2
Permanent marshes/waterbodies with low-density aquatic plants	0.2	757	0.5
Salt pan deep	−0.4	491	0.3
Salt pan shallow	−0.3	3	0.0
Seasonal wetland with high moisture	−0.1	4617	3.2
Seasonal wetland with low moisture	0.0	10461	7.2
Waterbody (fresh) deep	−0.3	11063	7.6
Waterbody (fresh) shallow	−0.1	1806	1.2

(*a*)

Figure 9. Wetland classes. (*a*) The dis-aggregated 15 class and (*b*) aggregated 8 class wetland classes determined based on the hierarchical classification system.

figure 8) using semi-automated techniques. The other 8 points that did not fall inside the wetlands were taken on narrow streams in hilly areas that were not recognizable in Landsat images. These were also areas where VFR imagery was absent to refine boundary delineation after the wetland digitization process (§2.6.3). The accuracy of 96.5% in wetland boundary delineation is remarkable, but achievable through semi-automated methods, especially when the VFR imagery (May *et al.* 2002, Fuller *et al.*

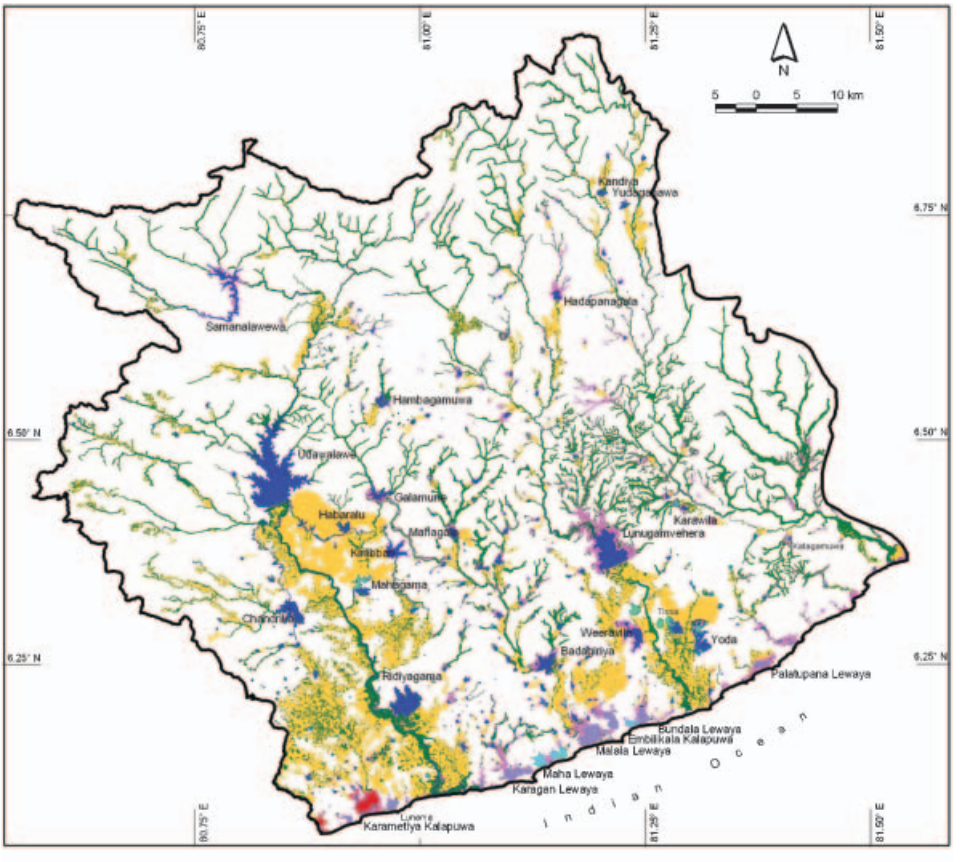

Basin boundary

Wetland types	Average NDVI (Dimensionless)	Area (Hectares)	Percentage
Irrigated agriculture	0.1	60406	41.5
Lagoon	−0.4	2141	1.5
Mangrove	0.2	624	0.4
Riparian vegetation and/or home garden	0.2	53042	36.4
Permanent marshes/waterbodies with aquatic plants	0.3	1079	0.7
Salt pan	−0.4	495	0.3
Seasonal wetlands	0.0	15077	10.4
Waterbody (fresh)	−0.3	12869	8.8

(*b*)

Figure 9. (*Continued*).

2006) is used to refine boundaries determined by Landsat ETM+ and the SRTM. The semi-automated methods require more time and resources than the automated methods, but the accuracies are way higher. Given that the precise delineation of the wetland boundaries is a must for wetland classification and characterization and since there is no automated methods (table 3) that can delineate wetlands accurately, the semi-automated methods are the best and the most accurate (table 5) option for wetland boundary delineation.

3.2.4 Wetland classes. Once the wetlands are delineated accurately (figure 8 and table 5), the classification of wetlands and the class identification and labelling

Table 5. Accuracies of wetland boundary delineation.

Number of wetland GT points	230
Number of GT points falling inside wetland boundary	222
Number of GT points falling outside wetland boundary	8
Overall accuracy (%)	96.5

process (figure 6, §2.6.4) leads to distinct classes (figures 9(*a*) and 9(*b*)). A hierarchical class labelling scheme, keeping in view of the recommendations by the Ramsar convention (Ramsar 2004), was adopted and wetlands were mapped at four levels (table 6): most disaggregated level I to most aggregated level IV. The class distribution for the most disaggregated level I (figure 9) and the aggregated level III (figure 10) show the dominance of irrigated areas (41.5%), natural vegetation and home gardens (36.4%) and seasonal wetlands (10.4%). An overwhelming proportion of the irrigated areas had rice cultivation.

3.2.5 Accuracies of wetland classes. The accuracies were assessed using the 115 independent data points reserved for the purpose. The wetland classes were mapped with an accuracy of 87% for 15 classes (figure 9) to 95% for 8 classes (figure 10 and table 7). The errors of commissions and the errors of omissions were low or negligible and those of K_{hat} (a measure of accuracy using Kappa Statistics) were high (table 7). These results clearly imply the strengths of the rigorous semi-automated methods and procedures adopted to identify and label wetland classes. However, it is possible to map more distinct wetland classes with lesser confusion and greater accuracies using the hyperspectral data (Hirano *et al.* 2003).

4. Wetland characterization

Once the classes are delineated and classified using fine resolution imagery, the class characteristics (e.g. figure 11) can be studied using MODIS monthly time-series MVC NDVI values as illustrated for the eight class map (figure 10). The NDVI time-series class characteristics follows the rainfall trend (figure 11); vegetation begins to gain vigour in mid September to October and remains at high vigour except for the months of mid May to mid September, where there are parched dry conditions (see figure 11). The trends of all classes follow a pattern with highest NDVI values for natural vegetation and irrigated agriculture and lowest for lagoons and salt pans (figure 11).

A major limitation of the Landsat ETM + and similar finer resolution data is the lack of time-series imagery. This is often a hindrance in understanding the land use/land cover (LULC) class characteristics. For example, Landsat ETM + can discern irrigated agriculture from mangrove forests and natural vegetation (see figure 9(*a*) and table 6). In contrast, the MODIS data fails to discern irrigated areas from natural vegetation and mangroves as a result of coarse 500 m spatial resolution. However, the continuous 8 day time-series data available from MODIS 7-band reflectance provides an invaluable understanding of the LULC characteristics. In this study, we demonstrated taking advantage of both higher spatial resolution Landsat ETM + to discern classes (figures 9(*a*) and 9(*b*) and table 6) and coarser spatial resolution MODIS 500 m data (figure 10). This is achieved through a three step process: (1) use Landsat ETM + to separate distinct classes, (2) mask out each class and cut out MODIS image areas coinciding with these class masks and (3) use MODIS NDVI MVC to generate time-series class characteristics (figure 10).

Table 6. Hierarchical classification of wetland classes at four levels.

Class no Level 1	Class name Level 1	Area (ha) Level 1	Class no Level 2	Class name Level 2	Area (ha) Level 2	Class no Level 3	Class name Level 3	Area (ha) Level 3	Class no Level 4	Class name Level 4	Area (ha) Level 4
1	Waterbody (fresh) deep	11096	1	Waterbody (fresh)	12940	1	Waterbody (fresh)	12940	1	Waterbody	15680
2	Waterbody (fresh) shallow	1843									
3	Lagoon deep	1810	2	Lagoon	2246	2	Waterbody (brackish)	2741			
4	Lagoon shallow	436									
5	Salt pan deep	491	3	Salt pan	495						
6	Salt pan shallow	3									
7	Seasonal wetland with high moisture	4923	4	Seasonal wetlands	16179	3	Seasonal wetlands	16179	2	Seasonal wetlands	16179
8	Seasonal wetland with low moisture	11255									
9	Permanent marshes/ waterbody with high-density vegetation	339	5	Permanent marshes/ water body with vegetation	1126	4	Permanent marshes/ water body with vegetation	1126	3	Vegetation	56094
10	Permanent marshes/ waterbody with low-density vegetation	788									
11	Mangrove high-density	461	6	Mangrove	734	5	Natural vegetation	54967			
12	Mangrove low-density	273									
13	Natural vegetation (riparian/homestead) high-density	32094	7	Natural vegetation (riparian/homestead)	54233						
14	Natural vegetation (riparian/homestead) low-density	22139									
15	Irrigated agriculture	62505	8	Irrigated agriculture	62505	6	Irrigated agriculture	62505	4	Irrigated agriculture	62505

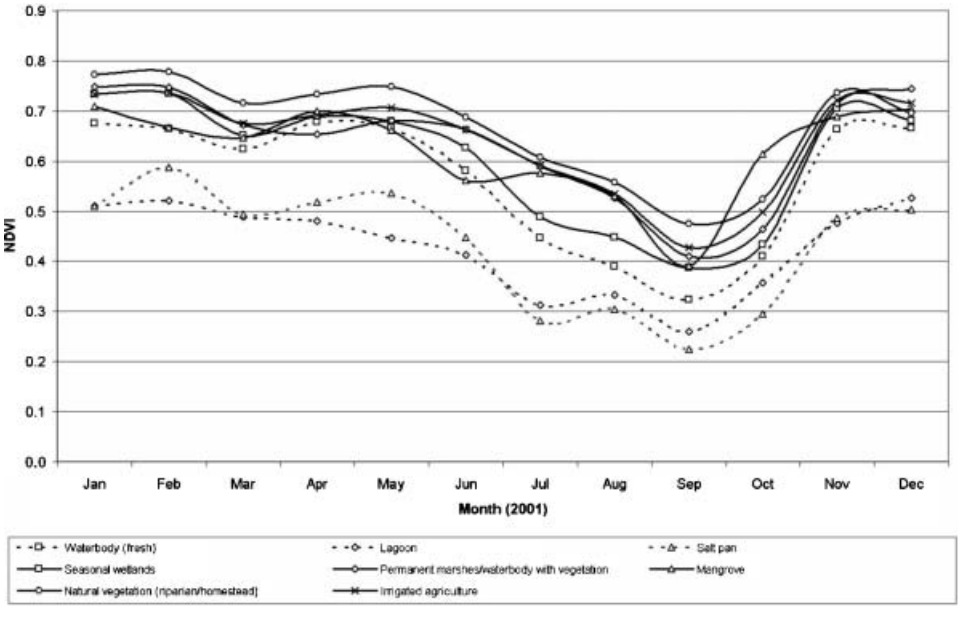

Figure 10. Characterization of wetlands. The time-series characteristics of various wetland classes as determined using MODIS NDVI MVC.

5. Conclusions

The study has established that the semi-automated methods involving image enhancement, display, digitizing and classifying techniques were very well suited for rapid and accurate delineation of wetlands using single date Landsat ETM+ and SRTM DEM data. The best Landsat ETM+ image enhancement and FCC RGB colour gun displays that help distinguish, digitize and delineate wetland boundaries from other land units were:

ETM+4/ETM+7, ETM+4/ETM+3, ETM+4/ETM+2,
ETM+4, ETM+3, ETM+5,
ETM+7, ETM+4, ETM+2 and
ETM+3, ETM+2, ETM+1.

In addition, the SRTM DEM slope of less than 1% also helped delineate large or higher order wetlands, rapidly and accurately.

Table 7. Accuracies and errors of wetland classes.

Classification level (no.)	Number of classes (no.)	Accuracy overall (%)	K_{hat} (Dimensionless)	Errors	
				Omission (%)	Commission (%)
1*	15	87	0.83	13	1
2	8	94	0.92	6	1
3	6	94	0.92	6	1
4	4	95	0.92	5	2

Note: * is accuracy assessment at level 1 and is reported for 13 out of 15 classes. Class numbers 6 and 12 did not have any ground truth data for accuracy assessment.

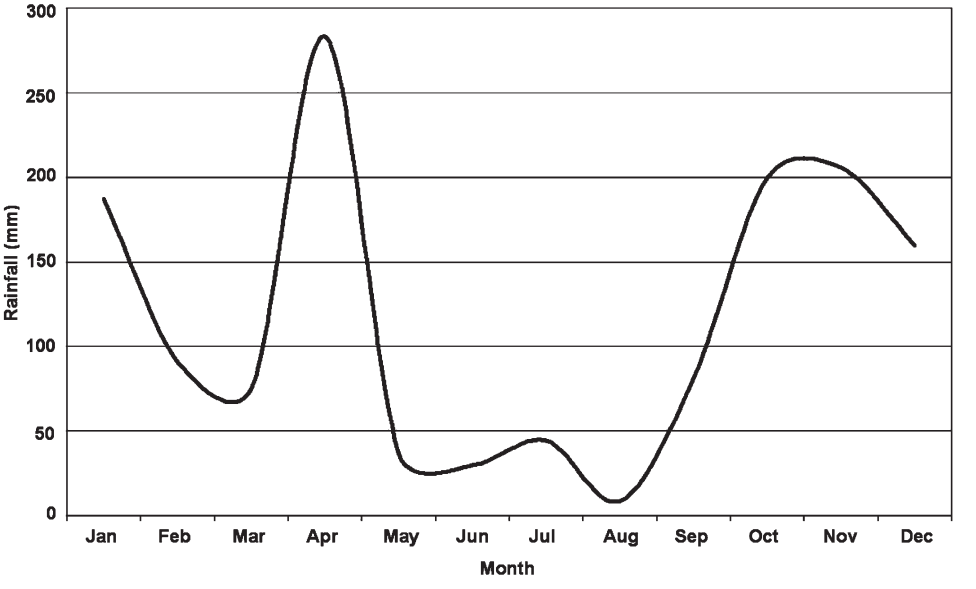

Figure 11. The bi-modal rainfall in the study area.

The strengths of the semi-automated methodologies were demonstrated in the Ruhuna river basin, Sri Lanka, which was a fairly large size basin with a total area of 608 000 ha and that had diverse climatic, topographic and biophysical conditions. The semi-automated techniques determined the wetlands to be 24% of the total basin area and were mapped at 97% accuracy, as determined using field-plot data. The high percentages of wetlands were mainly as a result of the 41% human-made irrigated areas, mostly under rice cultivation. Methods to establish different wetland classes were demonstrated using a hierarchical classification system. Fifteen disaggregated wetland classes were mapped with an accuracy of 87% (with a K_{hat} value of 0.83) and an error of omission of about 13% and error of commission of about 1%. For the aggregated 8, 6 and 4 classes, the accuracies were 94% or better (with K_{hat} of 0.92) with errors of omissions of about 6% and errors of commissions of about 1%.

In contrast, the automated methods of wetland delineation involving: (a) thresholds of Landsat ETM+ indices and wavebands, (b) SRTM-derived slopes, (c) algorithms for SRTM DEM-derived drainage delineation and (d) automated classification techniques, provided unacceptably low levels of accuracies and/or high levels of errors of omissions and/or commissions. Automated methods involving the SRTM-derived wetland boundaries had four known limitations: (a) churning out non-existent or spurious wetlands, (b) providing non-smooth alignment, (c) resulting in spatial dislocation of streams and (d) absence of stream width.

The study also demonstrated how the time-series MODIS 500 m data are used to characterize the wetland land use/land cover (LULC) classes derived using fine resolution Landsat ETM+ 30 m data. Thus, the higher resolution Landsat ETM+ and coarser resolution MODIS perfectly complement and supplement each other.

Acknowledgements

The funding for the project came from the International Water Management Institute (IWMI) core funds under the wetland project. The authors would like to

thank Professor Frank Rijsberman, Director-general of IWMI, for allocating funds. The work was carried out in collaboration with the Sri Lanka's Central Environmental Authority (CEA) and the World Conservation Union (IUCN). We especially want to thank Dr Ajith Rodrigo, Mr Ajith Gunawardana and Ms Chandani Edusuriya from CEA for participating in joint field work. We would also like to thank Dr Channa Bambaradeniya and Ms Asha de Vos from IUCN for extending their useful support for this project. Mr Sanjiv De Silva is thanked for project leadership and coordinating meetings. The excellent secretarial support of Ms Jacinthat Navarathne is much appreciated.

References

Baghdadi, N., Bernier, M., Gauthier, R. and Neeson, I., 2001, Evaluation of C-band SAR data for wetland mapping. *International Journal of Remote Sensing*, **22**, pp. 71–88.

Bourgeau-Chavez, L.L., Kasischke, E.S., Brunzell, S.M. and Mudd, J.P., 2001, Analysis of space-borne SAR data for wetland mapping in Virginia riparian ecosystems. *International Journal of Remote Sensing*, **22**, pp. 3665–3687.

Campbell, J.B., 2002, *Introduction to Remote Sensing* (London: Taylor and Francis).

Cowardin, L.M., Carter, V., Golet, F.C. and Laroe, E.T., 1979, *Classification of wetlands and deepwater habitats of the United States.* US Department of the Interior, Fish and Wildlife Service, Washington, DC (Jamestown, ND: Northern Prairie Wildlife Research Center Online). Available online at: http://www.npwrc.usgs.gov/resource/wetlands/classwet/index.htm (version 04 December 1998).

Crist, E.P. and Cicone, R.C., 1984, A physically-based transformation of thematic mapper data the TM tassel cap. *IEEE Transactions on Geoscience and Remote Sensing*, **22**, pp. 256–263.

Dwivedi, R.S., Rao, B.R.M. and Bhattacharya, S., 1999, Mapping wetlands of the Sundarban Delta and it's environs using ERS-1 SAR data. *International Journal of Remote Sensing*, **20**, pp. 2235–2247.

Earth Resources Digital Analysis System (ERDAS), 2006, Software help documentation.

Environmental System Research Institute (ESRI), 2001, Software help documentation.

Friedl, M.A., Muchoney, D., McIver, D., Gao, F., Hodges, J.F.C. and Strahler, A.H., 2000, Characterization of North American land cover from NOAA-AVHRR data using the EOS MODIS land cover classification algorithm. *Geophysical Research Letters*, **27**, pp. 977–980.

Fuller, L.M., Morgan, T.R. and Aichele, S.S., 2006, *Wetland delineation with IKONOS fine resolution satellite imagery*. Fort Custer Training Center, Battle Creek, MI. U.S. Geological Survey, Scientific Investigations Report 2006-5051. Available online at: http://pubs.water.usgs.gov/SIR2006-5051.

Harvey, K.R. and Hill, G.J.E., 2001, Vegetation mapping of a tropical freshwater swamp in the Northern Territory, Australia: a comparison of aerial photography, Landsat TM and SPOT satellite imagery. *International Journal of Remote Sensing*, **22**, pp. 2911–2925.

Hirano, A., Madden, M. and Welch, R., 2003, Hyperspectral image data for mapping wetland vegetation. *BioOne Journal*, **23**, pp. 436–448.

Jayatillake, H.M., 2002, Surface water resources of Ruhuna basins. In *World Water Assessment Programme, Sri Lanka Case Study, Ruhuna Basins, Workshop Proceedings*, 7–9 April 2002, Sri Lanka CSri Lanka: Ministry of Irrigation and Water Management).

Jensen, J.R., Rutchey, K., Koch, M.S. and Narumalani, S., 2002, Inland wetland change detection in the Everglades water conservation area 2A using a time series of normalized remotely sensed data. *Photogrammetric Engineering and Remote Sensing*, **61**, pp. 199–209.

KULAWARDHANA, R.W., THENKABAIL, P.S., VITHANAGE, J., BIRADAR, C., ISLAM MD., A., GUNASINGHE, S. and ALANKARA, R., 2007, Evaluation of the wetland mapping methods using Landsat ETM+ and SRTM Data. *Journal of Spatial Hydrology* (accepted).

LAN, Z. and ZHANG, D., 2006, Study on optimization-based layered classification for separation of wetlands. *International Journal of Remote Sensing*, **27**, pp. 1511–1520.

LUNETTA, R.S., BALOGH, M.E. and MERCHANT, J.W., 1999, Application of multi-temporal Landsat 5 TM imagery for wetland identification. *Photogrammetric Engineering and Remote Sensing*, **65**, pp. 1303–1310.

LYON, J.G., 2001, *Wetland Landscape Characterization: Techniques and Applications for GIS Mapping, Remote Sensing, and Image Analysis* (Michigan, USA: Ann Arbor Press).

LYON, J.G., YUAN, D. and LUNETTA, R.S., 1998, A change detection experiment using vegetation indices. *Photogrammetric Engineering and Remote Sensing*, **64**, pp. 143–150.

MAY, D., WANG, J., KOVACS, J. and MUTER, M., 2002, Mapping wetland extent using IKONOS satellite imagery of the O'Donnell point region, Georgian Bay, Ontario (London, Ontario, Canada: Department of Geography, University of Western Ontario).

MCLVER, D.K. and FRIEDL, M.A., 2002, Using prior probabilities in decision-tree classification of remotely sensed data. *Remote Sensing of Environment*, **81**, pp. 253–261.

OZESMI, S.L. and BAUER, M.E., 2002, Satellite remote sensing of wetlands. *Wetlands Ecology and Management*, **10**, pp. 381–402.

RAMSAR 2004, *The Ramsar Convention Manual: A Guide to the Convention on Wetlands (Ramsar, Iran, 1971)*, 3rd ed., RAMSAR Convention Secretariat, Gland, Switzerland. Available online at: http://www.ramsar.org/lib/lib_manual2004e.htm.

SADER, S.A., AHL, D. and WEN-SHU, L., 1995, Accuracy of Landsat-TM and GIS rule-based methods for forest wetland classification in Maine. *Remote Sensing of Environment*, **53**, pp. 133–144.

SCHOWENGERDT, R.A., 2007, *Remote Sensing: Models and Methods for Image Processing* (San Diego, CA: Academic Press (Elsevier)).

THENKABAIL, P.S. and NOLTE, C., 1995, *Mapping and Characterising Inland Valley Agroecosystems of West and Central Africa: A Methodology Integrating Remote Sensing, Global Positioning System, and Ground-Truth Data in a Geographic Information Systems Framework.* RCMD Monograph No. 16, International Institute of Tropical Agriculture, Ibadan, Nigeria.

THENKABAIL, P.S. and NOLTE, C., 1996, Capabilities of Landsat-5 Thematic Mapper (TM) data in regional mapping and characterization of inland valley agroecosystems in West Africa. *International Journal of Remote Sensing*, **17**, pp. 1505–1538.

THENKABAIL, P.S. and NOLTE, C., 2000, Regional characterisation of inland valley agroecosystems in west and central Africa using fine resolution remotely sensed data. In *GIS Applications for Water Resources and Watershed Management* (by J.G. Lyon), pp. 77–99 (London and New York: Taylor and Francis).

THENKABAIL, P.S., NOLTE, C. and LYON, J.G., 2000a, Remote sensing and GIS modeling for selection of benchmark research area in the inland valley agroecosystems of West and Central Africa. *Photogrammetric Engineering and Remote Sensing, Africa Applications Special Issue*, **66**, pp. 755–768.

THENKABAIL, P., SCHULL, M. and TURRAL, H., 2005, Ganges and Indus river basin land use/land cover (LULC) and irrigated area mapping using continuous streams of MODIS data. *Remote Sensing of Environment*, **95**, pp. 317–341.

THENKABAIL, P.S., SMITH, R.B. and DE-PAUW, E., 2000b, Hyperspectral vegetation indices for determining agricultural crop characteristics. *Remote sensing of Environment*, **71**, pp. 158–182.

THENKABAIL, P.S., SMITH, R.B. and DE-PAUW, E., 2002, Evaluation of narrowband and broadband vegetation indices for determining optimal hyperspectral wavebands for agricultural crop characterization. *Photogrammetric Engineering and Remote Sensing*, **68**, pp. 607–621.

THENKABAIL, P.S., BIRADAR, C.M., TURRAL, H., NOOJIPADY, P., LI, Y.J., VITHANAGE, J., DHEERAVATH, V., VELPURI, M., SCHULL, M., CAI, X.L. and DUTTA, R., 2006, *An Irrigated Area Map of the World (1999) Derived from Remote Sensing.* IWMI research report, International Water Management Institute, Colombo, Sri Lanka. Available online at: www.iwmigiam.org.

TOWNSEND, P.A. and WALSH, S.J., 1998, Modeling floodplain inundation using an integrated GIS with radar and optical remote sensing. *Geomorphology*, **21**, pp. 295–312.

TÖYRÄ, J., PIETRONIRO, A., MARTZ, L.W. and PROWSE, T.D., 1999, A multi-sensor approach to wetland flood monitoring (Canada: Department of Geography, University of Saskatchewan, Canada, John Wiley & Sons Ltd.), 16, pp. 1569–1581.